

---

---

# Quantitative PET Imaging Detects Early Metabolic Remodeling in a Mouse Model of Pressure-Overload Left Ventricular Hypertrophy In Vivo

Min Zhong<sup>1,2</sup>, Clayton E. Alonso<sup>2</sup>, Heinrich Taegtmeier<sup>3</sup>, and Bijoy K. Kundu<sup>2,4</sup>

<sup>1</sup>Department of Physics, University of Virginia, Charlottesville, Virginia; <sup>2</sup>Department of Radiology and Medical Imaging, University of Virginia, Charlottesville, Virginia; <sup>3</sup>Department of Internal Medicine, Division of Cardiology, University of Texas Medical School at Houston, Houston, Texas; and <sup>4</sup>Cardiovascular Research Center, University of Virginia, Charlottesville, Virginia

---

We proposed that metabolic remodeling in the form of increased uptake of the myocardial glucose analog <sup>18</sup>F-FDG precedes and triggers the onset of severe contractile dysfunction in pressure-overload left ventricular hypertrophy in vivo. To test this hypothesis, we used a mouse model of transverse aortic constriction (TAC) together with PET and assessed serial changes in cardiac metabolism and function over 7 d. **Methods:** Scans of 16 C57BL/6 male mice were obtained using a small-animal PET device under sevoflurane anesthesia. A 10-min transmission scan was followed by a 60-min dynamic <sup>18</sup>F-FDG PET scan with cardiac and respiratory gating. Blood glucose levels were measured before and after the emission scan. TAC and sham surgeries were performed after baseline imaging. Osmotic mini pumps containing either propranolol (5 mg/kg/d) or vehicle alone were implanted subcutaneously at the end of surgery. Subsequent scans were taken at days 1 and 7 after surgery. A compartment model, in which the blood input function with spillover and partial-volume corrections and the metabolic rate constants in a 3-compartment model are simultaneously estimated, was used to determine the net myocardial <sup>18</sup>F-FDG influx constant, *K<sub>i</sub>*. The rate of myocardial glucose utilization, rMGU, was also computed. Estimations of the ejection fractions were based on the high-resolution gated PET images. **Results:** Mice undergoing TAC surgery exhibited an increase in the *K<sub>i</sub>* (580%) and glucose utilization the day after surgery, indicating early adaptive response. On day 7, the ejection fraction had decreased by 24%, indicating a maladaptive response. Average *K<sub>i</sub>* increases were not linearly associated with increases in rMGU. *K<sub>i</sub>* exceeded rMGU by 29% in the TAC mice. TAC mice treated with propranolol attenuated the rate of <sup>18</sup>F-FDG uptake, diminished mismatch between *K<sub>i</sub>* and rMGU (9%), and rescued cardiac function. **Conclusion:** Metabolic maladaptation precedes the onset of severe contractile dysfunction. Both are prevented by treatment with propranolol. The early detection of metabolic remodeling may offer a metabolic target for modulation of hypertrophy.

**Key Words:** <sup>18</sup>F-FDG PET; glucose metabolism in heart; left ventricular ejection fraction; left ventricular hypertrophy

**J Nucl Med 2013; 54:609–615**

DOI: 10.2967/jnumed.112.108092

---

**M**yocardial hypertrophy is considered initially an adaptive response to stress. When stress is sustained, however, hypertrophy becomes maladaptive. Both functional and structural changes are accompanied by changes in energy substrate metabolism. A hallmark finding in myocardial hypertrophy is a shift away from fatty-acid to glucose oxidation (1). On the basis of earlier work ex vivo, we have proposed that this metabolic remodeling precedes as well as triggers left ventricular (LV) structural and functional remodeling in pressure-overload LV hypertrophy (LVH) and induces the fetal gene program (2–4). However, this hypothesis has never been evaluated in vivo. For this purpose, we used the mouse model of LV pressure overload after transverse aortic constriction (TAC) as a clinically relevant model to assess metabolism and function of the heart subjected to pressure overload using <sup>18</sup>F-FDG PET imaging.

A compartmental modeling technique was used to analyze images obtained dynamically to compute the rate of myocardial <sup>18</sup>F-FDG uptake and use. The quantification of these rates has been limited by the following 2 important factors: first, the limited spatial resolution of the small-animal PET scanners (5,6) leading to partial-volume (PV) effects, and second, the spillover of radioactivity from the blood pool to the myocardium, and vice versa. A major shortcoming of the image-derived blood input function (IDIF) method is that it is susceptible to spillover and PV effects (7).

In this study, a (compartment) model-corrected blood input function (MCBIF) was optimized, wherein the blood input function with spillover and PV corrections and the metabolic rate constants in a 3-compartment model were simultaneously estimated from ordered-subset expectation maximization maximum a posteriori (OSEM-MAP) cardiac and respiration-gated PET images with attenuation

---

Received May 2, 2012; revision accepted Nov. 12, 2012.

For correspondence or reprints contact: Bijoy K. Kundu, Department of Radiology and Medical Imaging, Cardiovascular Research Center, 409 Lane Rod., MR4, P.O. Box 801339, University of Virginia, Charlottesville, VA 22908.

E-mail: bkk5a@virginia.edu

Published online Feb. 20, 2013.

COPYRIGHT © 2013 by the Society of Nuclear Medicine and Molecular Imaging, Inc.

correction (8). LV ejection fraction (LVEF) was also measured using high-resolution gated PET images, enabling us to perform a side-by-side comparison of cardiac metabolism and LV function.

## MATERIALS AND METHODS

### Animal Model

Sixteen adult C57BL/6 male mice (age, 9–10 wk) obtained from Charles River were imaged at baseline using a microPET Focus-F120 scanner (Siemens, Inc.) under sevoflurane anesthesia (9). A subset of these mice ( $n = 11$ ) was subjected to a TAC surgical procedure to induce pressure-overload hypertrophy (10). Briefly, mice were anesthetized with isoflurane and intubated for ventilation. A thoracotomy was performed, and a 7-0 silk suture was tied around the transverse aorta between the proximal and distal carotid arteries against a 27-gauge needle, after which, the needle was removed. Osmotic mini pumps containing either propranolol (5 mg/kg/d; Sigma Aldrich Inc.) ( $n = 6$ ) or vehicle alone ( $n = 5$ ) were implanted subcutaneously at the end of surgery. In addition, 5 sham-operated animals were subjected to the same surgical protocol, without tying off the suture. Before and after surgery, all mice were kept in an environment of 12-h light/12-h dark. Before imaging, animals were (11) overnight with access only to water.

PET scans were obtained between 9 AM and 5 PM on anesthetized animals. All experiments were performed in compliance with the *Guide for the Care and Use of Laboratory Animals* (12) and were conducted under protocols approved by the Institutional Animal Care and Use Committee at the University of Virginia.

### Small-Animal PET Imaging

PET imaging for measuring myocardial  $^{18}\text{F}$ -FDG uptake and glucose utilization was performed using  $^{18}\text{F}$ -FDG in the sham mice, TAC mice, and TAC mice treated with propranolol as follows: after the insertion of a tail-vein catheter, electrocardiograph surface electrodes (Blue Sensor; Ambu Inc.) were placed on both forepaws and the left hind paw, and a pneumatic respiratory pillow was placed on the animal's chest. Dynamic PET scans (60 min) were obtained under 2.5% sevoflurane anesthesia in oxygen (9), where data acquisition was initiated a few seconds before the slow administration of about 29.6 MBq (800  $\mu\text{Ci}$ ) of  $^{18}\text{F}$ -FDG over 30–60 s via the catheter. A Small Animal Monitoring and Gating System (model 1025 L; Small Animal Instruments, Inc.) for PET imaging was used to continuously monitor heart rate, respiration, and core body temperature (rectal probe). Cardiac gate signals were generated at the end-expiration phase of the respiratory cycle to time-stamp the PET scanner data for subsequent retrospective reordering into heart- and respiratory-cycle-based time bins (13). Transmission scans using a  $^{57}\text{Co}$  point source were obtained for attenuation correction before  $^{18}\text{F}$ -FDG administration. The list-mode data (sorted into 23 time bins [ $11 \times 8$ ,  $1 \times 12$ ,  $2 \times 60$ ,  $1 \times 180$ , and  $8 \times 400$  s]) and 3 gates [hence referred to as gated]) were reconstructed using an OSEM-MAP algorithm (14,15) with attenuation correction. For comparison the data were also reconstructed using a filtered backprojection (FBP) algorithm (ramp filter cut off at the Nyquist frequency) with the same spatial resolution without gating. The images were corrected for radioactive decay, random coincidences, and dead-time losses using the microPET Manager (Siemens Inc.). Regions of interest in the area corresponding to the LV blood pool and the myocardium were drawn in the last frame and the last gate of the dynamic image data, and time-activity curves for the LV blood pool and the myocardium were generated for the whole scan duration of 60 min. Blood samples were also

collected at around 43 and 56 min after  $^{18}\text{F}$ -FDG administration from the tail vein to validate the MCBIF. Three blood samples before and 3 blood samples after the PET scan were drawn by a tail-vein nick to measure blood glucose levels using a glucometer (Accu-Chek; Roche). The average of these blood glucose readings was used to compute the rate of myocardial glucose utilization (rMGU).

An MCBIF (8,16), based on the simultaneous estimation of the blood input function with spillover and PV corrections and the metabolic rate constants, was optimized in this study. The formalism for MCBIF was used to measure the net myocardial  $^{18}\text{F}$ -FDG influx,  $K_i$ , and hence glucose utilization, rMGU, in vivo in the sham mice, TAC mice, and TAC mice treated with propranolol.

End-systolic volumes (ESV) and end-diastolic volumes (EDV) were also measured by drawing regions of interest at the end-systolic and end-diastolic phases of the heart cycle over multiple slices covering the whole heart from the apex to the base. The volumes obtained in each phase over multiple slices were summed to obtain net ESV and EDV in microliters ( $\mu\text{L}$ ). The LVEF was measured by the following equation:  $(\text{EDV} - \text{ESV})/(\text{EDV}) \times 100\%$ .

### MCBIF

On the basis of the 3-compartment  $^{18}\text{F}$ -FDG model (Fig. 1), the differential equations for  $^{18}\text{F}$ -FDG kinetics can be written as follows (17):

$$dC_e/dt = K_1 C_p(t) - (k_2 + k_3) C_e(t) + k_4 C_m(t) \quad (\text{Eq. 1})$$

$$dC_m/dt = k_3 C_e(t) - k_4 C_m(t), \quad (\text{Eq. 2})$$

where the 3 compartments are  $C_p(t)$  (the  $^{18}\text{F}$ -FDG concentration in the blood compartment),  $C_e(t)$  (the concentration of  $^{18}\text{F}$ -FDG in the interstitial and cellular spaces), and  $C_m(t)$  (the  $^{18}\text{F}$ -FDG concentration within the cell of the phosphorylated FDG-6-phosphate).  $K_1$  and  $k_2$  are the forward rate constant and reverse rate constant, respectively, between the first 2 compartments.  $k_3$  and  $k_4$  are the rates of phosphorylation and dephosphorylation between compartments 2 and 3.  $C_e(t)$  and  $C_m(t)$  can be solved in terms of  $C_p(t)$  and the rate constants,  $K_1$ – $k_4$ ,

$$C_T(t) = \frac{K_1}{a_1 - a_2} \times [(k_3 + k_4 - a_1) e^{-a_1 t} + (a_2 - k_3 - k_4) e^{-a_2 t}] \otimes C_p(t), \quad (\text{Eq. 3})$$

where

$$a_{2,1} = 1/2 \left( k_2 + k_3 + k_4 \pm \sqrt{(k_2 + k_3 + k_4)^2 - 4k_2 k_4} \right) \quad (\text{Eq. 4})$$

and

$$C_T(t) = C_e(t) + C_m(t) \quad (\text{Eq. 5})$$

is the net myocardium tissue concentration (Fig. 1). Assuming the rate of dephosphorylation,  $k_4 = 0$ , the net myocardial  $^{18}\text{F}$ -FDG influx constant,  $K_i$ , can be written as

$$K_i = K_1 \frac{k_3}{(k_2 + k_3)}. \quad (\text{Eq. 6})$$

Ideally, when a region of interest is drawn within the cavity of the left ventricle, the tissue time-activity curve would equal the

whole-blood time–activity curve  $C_p$ . However, because of spillover and PV effects, the model equation for an image-derived time–activity curve from the blood pool can be written in terms of fraction of the tissue concentration in the blood compartment and partial recovery of radioactivity concentration from the blood as:

$$Model_{IDIF,i} = \frac{\int_{t_b^i}^{t_e^i} [S_{mb}(C_T(t)) + r_b C_p] dt}{t_e^i - t_b^i}. \quad (\text{Eq. 7})$$

Similarly, for the myocardium tissue, one can write the model equation as:

$$Model_{myo,i} = \frac{\int_{t_b^i}^{t_e^i} [r_m C_T(t) + S_{bm} C_p] dt}{t_e^i - t_b^i}, \quad (\text{Eq. 8})$$

where  $r_m$  and  $r_b$  are the recovery coefficients (accounting for PV effect) for the myocardium and blood pool, respectively.  $S_{bm}$  and  $S_{mb}$  are the spillover coefficients from the blood pool to the myocardium and vice versa, respectively.  $t_b^i$  and  $t_e^i$  are the beginning and end times, respectively, for a single frame in a dynamic PET scan. The model equation for the blood input function can be written as (18):

$$C_p(t) = (A_1(t - \tau) - A_2 - A_3)e^{L_1(t - \tau)} + A_2e^{L_2(t - \tau)} + A_3e^{L_3(t - \tau)}, \quad (\text{Eq. 9})$$

where the terms associated with  $A_1$ ,  $A_2$ , and  $A_3$ , respectively represent the amplitude, falling edge, and washout of the tracer over time. By substituting Equations 3 and 9 in Equations 7 and 8, we can optimize the model equations to the blood ( $PET_{IDIF}$ ) and tissue ( $PET_{myo}$ ) time–activity curves obtained from OSEM-MAP cardiac and respiration-gated PET images with attenuation correction as indicated below:

$$O(p) = \sum_{i=1}^n [(Model_{IDIF,i} - PET_{IDF,i})^2 + (Model_{myo,i} - PET_{myo,i})^2]. \quad (\text{Eq. 10})$$

The optimization was performed by minimizing the objective function (Eq. 10) in the MATLAB programming environment using the function “fmincon,” which is based on an interior-reflective Newton method. The initial guesses and bounds for the PV averaging coefficients ( $r_m$ ,  $r_b$ ) are determined beforehand by performing

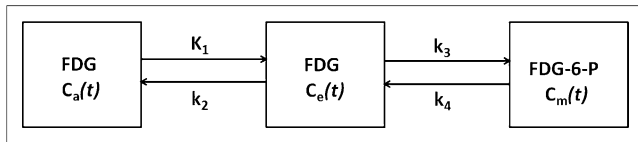


**FIGURE 1.** Three-compartment  $^{18}\text{F}$ -FDG model. Block diagram indicates rate constants  $K_1$ – $k_4$ , between 3 compartments of  $^{18}\text{F}$ -FDG kinetic model. Left compartment is vascular space for  $^{18}\text{F}$ -FDG,  $C_a$ . Middle compartment is extravascular space for  $^{18}\text{F}$ -FDG,  $C_e$ . Right compartment is cellular space for phosphorylated FDG-6-phosphate (FDG-6-P),  $C_m$ . Second and third compartments add up to form myocardial tissue compartment,  $C_T$ .

phantom experiments (14). We have kept the bounds for all the kinetic parameters ( $K_1$ – $k_4$ ) and spillover factors ( $S_{bm}$ ,  $S_{mb}$ ) open between 0 and 1. As for the input function, one side of the bounds is determined by the distribution of the input function ( $A_1, A_2, A_3 > 0$  and  $L_1, L_2, L_3 < 0$ ) whereas the other side is wide open. Optimization of Equation 10 results in simultaneous estimation of the blood input function, Equation 9, and compartment model parameters  $K_1$ – $k_4$  and hence Ki along with the spillover and PV coefficients ( $S_{mb}$ ,  $r_b$ ,  $S_{bm}$ ,  $r_m$ ), without the need for any blood sampling. Simultaneous estimation results in the blood input function, Equation 9, to be free of spillover contamination and PV-corrected in a 3-compartment model. The rate of myocardial glucose utilization can then be computed as:

$$rMGU = K_i[Glu]/LC, \quad (\text{Eq. 11})$$

in  $\mu\text{mol/g/min}$ , where  $[Glu]$  is the average nonradioactive blood glucose levels measured using a glucometer and  $LC$  is the lumped constant. The  $LC$  corrects the difference of affinity between glucose and  $^{18}\text{F}$ -FDG to glucose transporters and the phosphorylating system. In recent years, the value of the  $LC$  has been questioned, and it is uncertain which value should be used (19–22). In the 3-compartment model of glucose transfer into cells, the  $LC$  is a function of the correlation between the net and the unidirectional rates of uptake of glucose and glucose tracers such as  $^{18}\text{F}$ -FDG. For the sake of simplicity, we, like many investigators, have used an  $LC$  of 1 (23,24).

### Statistical Analysis

Statistical analysis was performed using SigmaStat 3.0 (SPSS, Inc.). Mean values of Ki,  $[Glu]$ , rMGU, and LVEF were calculated with SE. Two-way repeated-measures ANOVA and Holm–Sidak post hoc tests were used to compare mean values in the sham mice, TAC mice, and TAC mice treated with propranolol at different time points. A  $P$  value of less than 0.05 was considered statistically significant.

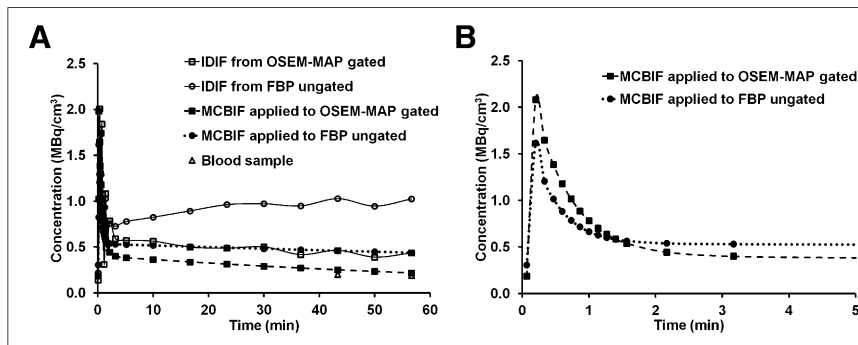
## RESULTS

### Quantitative Accuracy of MCBIF Applied to IDIF from OSEM-MAP Gated Images

Representative IDIFs obtained from OSEM-MAP gated images and from FBP ungated images with attenuation correction are shown in Figure 2A. MCBIF applied to IDIF obtained from OSEM-MAP gated and FBP ungated images are also shown in the figure. The venous blood samples at 43 and 56 min are shown for comparison. MCBIF applied to the IDIF obtained from high-resolution gated images correctly accounted for the washout dynamics of  $^{18}\text{F}$ -FDG from the blood, when compared with the late venous blood samples. Figure 2B shows MCBIF estimation during the first 5 min of the scan, indicating improved PV recovery when applied to IDIF obtained from OSEM-MAP gated images as compared with that obtained from ungated FBP images.

A residual plot of MCBIF applied to high-resolution gated images, when compared with the 2 late venous blood samples obtained from control mice ( $n = 6$ ), is shown in Figure 3. The analysis revealed an average difference of  $0.017 \text{ MBq/cm}^3$ . The precision (SD of differences) was  $0.13 \text{ MBq/cm}^3$ . The figure also shows the analysis obtained

**FIGURE 2.** (A) MCBIF estimation for whole scan duration. Shown are representative IDIFs obtained from OSEM-MAP cardiac- and respiration-gated images and from FBP ungated images with attenuation correction. MCBIF applied to IDIF from OSEM-MAP gated and FBP ungated images is also shown. Venous blood samples at around 43 and 56 min are shown for comparison. MCBIF applied to IDIF obtained from high-resolution gated images correctly accounts for washout dynamics of  $^{18}\text{F}$ -FDG from blood, when compared with late venous blood samples. (B) MCBIF estimation during first 5 min of scan. Scan indicates improved PV recovery when applied to IDIF obtained from OSEM-MAP gated images as compared with that obtained from ungated FBP images.



from FBP ungated images. The plot indicated the average difference and precision obtained from the FBP ungated dataset to be  $0.28 \text{ MBq/cm}^3$  and  $0.33 \text{ MBq/cm}^3$ , respectively. The residual plot exhibits the quantitative accuracy and repetitive behavior of MCBIF when applied to OSEM-MAP gated images.

### Metabolic Remodeling in LVH in Mice in Vivo

Figure 4 shows representative gated transverse PET images at the last time bin for the sham mice, TAC mice, and TAC mice treated with propranolol at baseline, day 1, and day 7 after surgery. All scans are from the same animals. The images indicate an enlargement in the LV cavity over a period of 7 d in the TAC mice. The images also show an increase in  $^{18}\text{F}$ -FDG uptake in the TAC mice starting at day 1 indicative of metabolic adaptation in pressure-overload LVH.

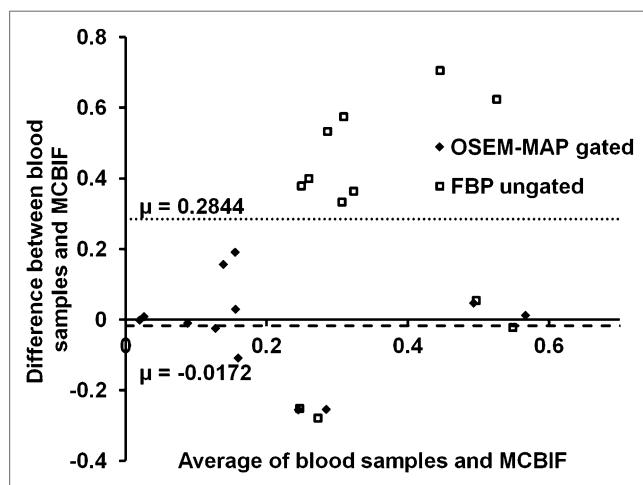


**FIGURE 3.** Residual plot. MCBIF applied to high-resolution gated images, when compared with 2 late venous blood samples, revealed average difference of  $0.017 \text{ MBq/cm}^3$  in control mice ( $n = 6$ ). Precision (SD of differences) was  $0.13 \text{ MBq/cm}^3$ . Figure also shows analysis obtained from FBP ungated images. Plot indicated average difference and precision to be  $0.28$  and  $0.33 \text{ MBq/cm}^3$ , respectively, obtained from FBP ungated datasets. Residual plot indicates quantitative accuracy and repetitive behavior of MCBIF applied to OSEM-MAP gated images.

The measured rate of myocardial  $^{18}\text{F}$ -FDG uptake,  $K_i$  ( $\text{mL/g/min}$ ), for the mice in the 3 categories is shown in Figure 5A over a period of 7 d. The plot shows increased myocardial  $^{18}\text{F}$ -FDG uptake at day 1 after TAC surgery by 580%, indicating an adaptive response with preserved LVEF (Fig. 5B).  $K_i$  increased further at day 7, with a drop in function by 24%. The blood glucose levels and rMGU are also shown in Figures 6A and 6B for the 3 categories over a period of 7 d. We observed a drop in blood glucose levels at day 1 for the sham mice, TAC mice, and TAC mice treated with propranolol. Mice treated with propranolol showed an elevation in blood glucose levels at day 7, significantly different from day 1 and comparable to the sham group or mice at baseline. The TAC mice exhibited an insignificant increase in blood glucose levels between days 1 and 7 (Fig. 6A). The rMGU (Fig. 6B) did not increase linearly with  $K_i$ . Rather, rMGU increased at a much slower rate than  $K_i$ , thereby resulting in a mismatch of 29% between  $K_i$  and rMGU in the TAC mice (Fig. 7). On the other hand, early treatment with propranolol (25) targeting metabolic alterations served to attenuate the rate of myocardial  $^{18}\text{F}$ -FDG uptake (Fig. 5A) reduce mismatch between  $K_i$  and rMGU to 9%, and rescue cardiac function (Fig. 5B). The metabolic changes and cardiac function in the TAC mice treated with propranolol were comparable to those in the sham group. The in vivo imaging results suggest that early metabolic remodeling may precede and trigger the onset of severe contractile dysfunction in LVH in mice.

### DISCUSSION

In the normal heart, fatty acid oxidation is the predominant source (60%–90%) of adenosine triphosphate, with glucose oxidation and lactate contributing the rest (26). Stress on the myocardium, such as biomechanical stress from pressure overload, changes normal myocardial substrate metabolism. In the case of pressure-overload-induced hypertrophy, the prevailing notion is that alterations in energy substrate metabolism adversely affect the response to myocardial ischemic stresses and contribute to contractile dysfunction. Specifically, in the hypertrophic heart there is a shift away from fatty acid oxidation toward glucose metabolism (1). At least initially,

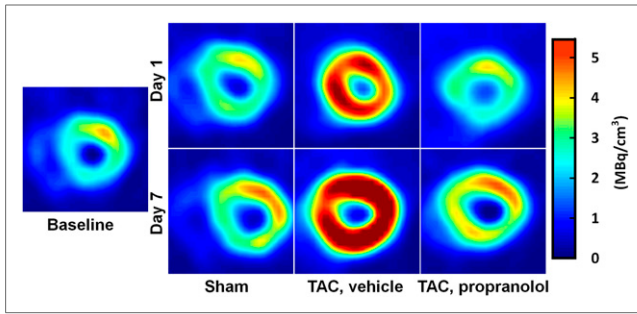


**FIGURE 4.** Gated transverse PET images in vivo. End-diastolic transverse PET images at last time bin for sham mice, TAC mice, and TAC mice treated with propranolol at baseline, day 1, and day 7 after surgery are shown. All scans are from same animals. Images indicate enlargement in LV cavity in TAC mice over 7 d. Images also show increase in  $^{18}\text{F}$ -FDG uptake in TAC mice starting at day 1, indicative of metabolic adaptation in pressure-overload LVH.

this metabolic remodeling may be considered as adaptive, most likely because glucose oxidation yields more adenosine triphosphate per atom of oxygen (2). With time, however, the adaptive response becomes maladaptive because this shift in metabolism does not increase adenosine triphosphate production commensurate with the increased demand for energy by the heart.

Recently, we have proposed a requirement for hexose 6-phosphate in mammalian-target-of-rapamycin signaling and cardiac growth (27). However, in the setting of insulin resistance, an oversupply of substrate (glucose) may “starve the heart in the midst of plenty” (28). The hypothesis, however, has never been tested serially in vivo because of the limited availability of technologies for studying complex metabolic parameters and LV function. It is tempting to speculate that strategies to improve myocardial substrate use and to improve metabolic flexibility (3,29) in the hypertrophic heart may improve contractile performance and prevent the onset of heart failure.

During acute pressure overload and inotropic stimulation (30), glucose oxidation is increased, but it is not yet completely clear how glucose uptake is related to LV function

during pressure-overload LVH. Studies using SPECT imaging have demonstrated that the metabolic switch can be measured in both small animals and human beings (31,32). However, a serial study on the temporal relationship between glucose uptake and cardiac function in vivo in mice using PET has not been done. We demonstrated that MCBIF applied to an IDIF obtained from high-resolution gated images with less severe spillover and PV effects is quantitative and also repetitive as compared with that obtained from low-resolution ungated images (16). The results of our present study support the hypothesis that an increase in glucose metabolism in the form of increased  $^{18}\text{F}$ -FDG uptake precedes and triggers the onset of severe dysfunction of the heart in LVH. This finding is important because early detection of metabolic remodeling may lead to early intervention targeting metabolic changes to prevent the onset of severe contractile dysfunction and improve patient outcomes clinically. We also observed that early treatment with propranolol served to attenuate myocardial glucose uptake and rescue cardiac function in vivo. Thus, metabolic imaging with  $^{18}\text{F}$ -FDG PET may provide an early indication of a beneficial effect of a therapy, possibly presenting a platform for aggressive treatment strategies to improve outcomes clinically.

Dietary conditions affect  $^{18}\text{F}$ -FDG PET imaging studies (33). Some clinical studies use glucose load conditions without fasting to obtain higher-quality images. On the other hand, fasting can produce similar-quality images. Because we are interested in  $^{18}\text{F}$ -FDG dynamics, a reasonable contrast between the blood pool and the myocardial tissue enables us to draw regions of interest and determine rate of myocardial  $^{18}\text{F}$ -FDG influx with spillover and PV corrections. Moreover, performing glucose clamping in addition to the TAC surgery in mice is challenging, thus we resort to overnight fasting for our  $^{18}\text{F}$ -FDG PET scans to achieve uniform metabolic conditions to obtain  $K_i$  and rMGU.

The  $LC$  is an important parameter in the determination of the rMGU in a dynamic PET scan. This value may vary, depending on plasma substrate and hormonal conditions. Many authors have used a constant value of  $LC$  to compute

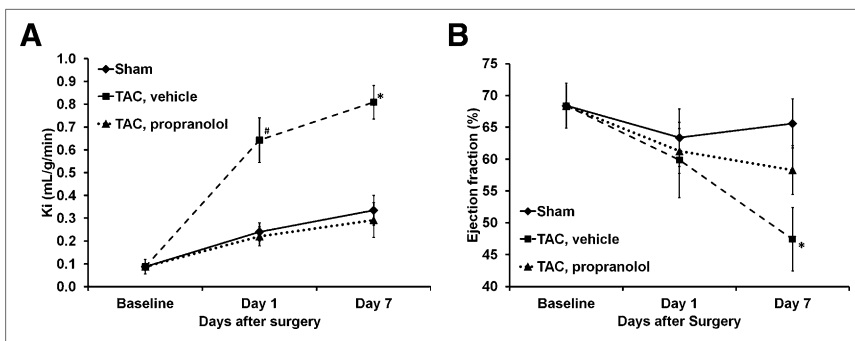
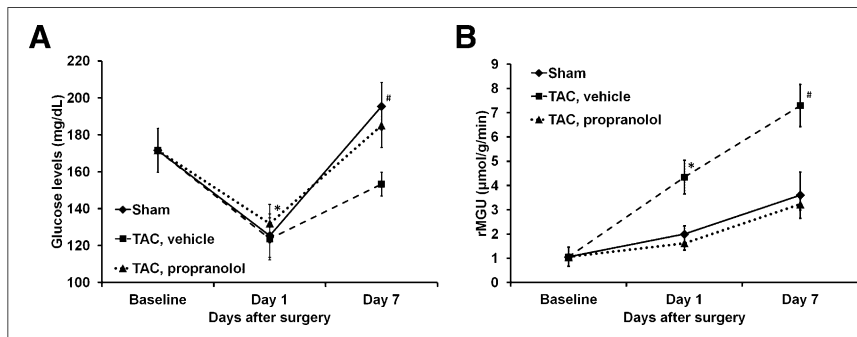


**FIGURE 5.** (A) Measured rates of myocardial  $^{18}\text{F}$ -FDG uptake in vivo.  $K_i$  (mL/g/min) for sham mice ( $n = 5$ ), TAC mice, vehicle ( $n = 5$ ) mice, and TAC mice treated with propranolol ( $n = 6$ ) are shown. Myocardial  $^{18}\text{F}$ -FDG uptake at day 1 after TAC surgery is increased by 580%, indicating adaptive response to stress.  $K_i$  increased further on day 7 in TAC mice, whereas TAC mice treated with propranolol exhibited attenuated rate of myocardial  $^{18}\text{F}$ -FDG uptake over 7-d period. Metabolic changes in TAC mice treated with propranolol were comparable

to sham group. All values are mean  $\pm$  SEM. (B) Measured LVEF from dynamic gated PET images in vivo. Plot indicates insignificant drop in function in TAC mice on day 1. On day 7, function dropped by 24% in TAC mice whereas there is insignificant drop in function in TAC mice treated with propranolol. Sham group indicates no significant change in function over 7-d period. All values are mean  $\pm$  SEM.  $^{*}P < 0.05$  vs. baseline, TAC treated with propranolol, and sham groups.

**FIGURE 6.** (A) Blood glucose levels. Plot shows average blood glucose levels measured at each time point for sham mice, TAC mice, and TAC mice treated with propranolol. All values are mean  $\pm$  SEM. \* $P < 0.05$  vs. BSL and day 1. # $P < 0.05$  vs. TAC at day 7. (B) rMGU was measured at each time point for sham mice, TAC mice, and TAC mice treated with propranolol. All values are mean  $\pm$  SEM. \* $P < 0.05$  vs BSL, day 1, TAC treated with propranolol, and sham groups. # $P < 0.05$  vs baseline, TAC treated with propranolol, and sham groups.



myocardial glucose utilization in humans with type 2 diabetes (34). Botker et al. (35) proposed that  $LC$  is a function of rates of  $^{18}\text{F}$ -FDG transport and phosphorylation and applied the method to assess myocardial glucose utilization in humans with ischemic cardiomyopathy (36). In a study by Herrero et al. (37), a constant value of  $LC$  was used for assessing myocardial glucose utilization for  $^{18}\text{F}$ -FDG PET studies in dogs. However, they also observed that the correlation between Fick-derived and PET-derived rMGU has a lower correlation with the variable  $LC$ . The correlation coefficient does not differ after correcting for an  $LC$  of 0.67 for  $^{18}\text{F}$ -FDG PET studies. In addition, they noted that using the variable  $LC$  leads to a significant underestimation of rMGU in large animals. In the current work, we used an  $LC$  of 1 because we did not measure this constant and there is no consensus on how to deal with this issue. The concerns expressed earlier by Botker et al. (35) do not apply because here the metabolic conditions were the same for all animals and in steady state. Nevertheless, further studies need to be done to characterize  $LC$  in small-animal PET imaging of the heart.

Our study was not without limitations. First,  $^{18}\text{F}$ -FDG can be considered only as a surrogate marker for glucose metabolism. Although  $^{18}\text{F}$ -FDG indirectly assesses glucose

transport and phosphorylation, the tracer analog is subjected to changes in the  $LC$  (19). Second, although clinically relevant, the acute nature of the model might have been a limitation in evaluating the hypothesis of metabolic remodeling that precedes and triggers cardiac dysfunction in LVH. The slowly progressive Dahl salt-sensitive hypertensive rat model may be more relevant to evaluate metabolic and functional changes in the heart, in vivo, but the costs for a study such as the present one would be prohibitive (38). Using the 1-kidney, 1-clip rabbit model of hypertension, we have already shown by invasive measurements that metabolic remodeling of the heart precedes hypertrophy (2). Third, we did not consider any possible differences in plasma substrate or hormone levels, although all scans were obtained under the same conditions and any errors would be systematic errors.

## CONCLUSION

Noninvasive serial imaging of the heart subjected to pressure-overload hypertrophy using PET supports the hypothesis that changes in the glucose analog  $^{18}\text{F}$ -FDG metabolism precede and trigger the onset of severe cardiac dysfunction in LVH. We found that enhanced uptake of  $^{18}\text{F}$ -FDG by the myocardium in mice subjected to pressure-overload hypertrophy precedes and possibly triggers the onset of contractile dysfunction. Early intervention with a standard-of-care treatment prevented maladaptive response and rescued cardiac function. We speculate that early detection of metabolic remodeling may offer a metabolic target for modulation of hypertrophy.

## DISCLOSURE

The costs of publication of this article were defrayed in part by the payment of page charges. Therefore, and solely to indicate this fact, this article is hereby marked "advertisement" in accordance with 18 USC section 1734. This work was supported by grants HL 102627 and HL 61483 from the U.S. Public Health Service. No other potential conflict of interest relevant to this article was reported.

## ACKNOWLEDGMENTS

We thank Barbara Thornhill for performing the animal surgeries and Gina Wimer for the tail-vein injections during the course of the study.

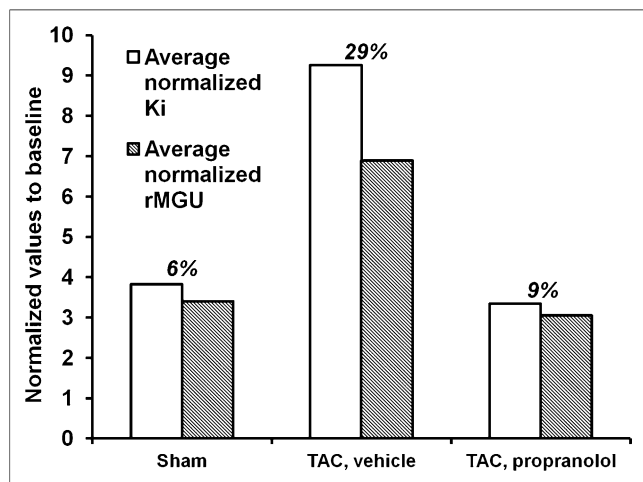


**FIGURE 7.** Comparison between  $K_i$  and rMGU measured in vivo at day 7. rMGU did not increase linearly with  $K_i$ . rMGU increased at much slower rate than  $K_i$ , resulting in mismatch of 29% between  $K_i$  and rMGU in TAC mice. Treatment with propranolol reduced mismatch to 9% and rescued cardiac function.

## REFERENCES

- Bishop SP, Altschuld RA. Increased glycolytic metabolism in cardiac hypertrophy and congestive failure. *Am J Physiol.* 1970;218:153–159.
- Taegtmeier H, Overturf ML. Effects of moderate hypertension on cardiac function and metabolism in the rabbit. *Hypertension.* 1988;11:416–426.
- Taegtmeier H, Golfman L, Sharma S, et al. Linking gene expression to function: Metabolic flexibility in the normal and diseased heart. *Ann N Y Acad Sci.* 2004;1015:202–213.
- Taegtmeier H, Sen S, Vela D. Return to the fetal gene program: a suggested metabolic link to gene expression in the heart. *Ann N Y Acad Sci.* 2010;1188:191–198.
- Tai YC, Ruangma A, Rowland D, et al. Performance evaluation of the microPET focus: a third-generation microPET scanner dedicated to animal imaging. *J Nucl Med.* 2005;46:455–463.
- Tai YC, Chatziioannou AF, Yang Y, et al. MicroPET II: design, development and initial performance of an improved microPET scanner for small-animal imaging. *Phys Med Biol.* 2003;48:1519–1537.
- Laforest R, Sharp TL, Engelbach JA, et al. Measurement of input functions in rodents: challenges and solutions. *Nucl Med Biol.* 2005;32:679–685.
- Zhong M, Locke LW, Kundu BK. Compartment model corrected blood input function estimate improves with iterative image reconstruction algorithm and cardiac gating [abstract]. *J Nucl Med.* 2011;52(suppl 1):2104.
- Flores JE, McFarland LM, Vanderbilt A, et al. The effects of anesthetic agent and carrier gas on blood glucose and tissue uptake in mice undergoing dynamic FDG-PET imaging: sevoflurane and isoflurane compared in air and in oxygen. *Mol Imaging Biol.* 2008;10:192–200.
- Liao Y, Ishikura F, Beppu S, et al. Echocardiographic assessment of LV hypertrophy and function in aortic-banded mice: necropsy validation. *Am J Physiol Heart Circ Physiol.* 2002;282:H1703–H1708.
- Lee KH, Ko BH, Paik JY, et al. Effects of anesthetic agents and fasting duration on F-18-FDG biodistribution and insulin levels in tumor-bearing mice. *J Nucl Med.* 2005;46:1531–1536.
- Guide for the Care and Use of Laboratory Animals.* 8th ed. Washington, DC: National Academy Press; 2010.
- Yang Y, Rendig S, Siegel S, et al. Cardiac PET imaging in mice with simultaneous cardiac and respiratory gating. *Phys Med Biol.* 2005;50:2979–2989.
- Locke LW, Berr SS, Kundu BK. Image-derived input function from cardiac gated maximum a posteriori reconstructed PET images in mice. *Mol Imaging Biol.* 2011;13:342–347.
- Qi J, Leahy RM, Cherry SR, et al. High-resolution 3D Bayesian image reconstruction using the microPET small-animal scanner. *Phys Med Biol.* 1998;43:1001–1013.
- Fang YH, Muzic RF Jr. Spillover and partial-volume correction for image-derived input functions for small-animal <sup>18</sup>F-FDG PET studies. *J Nucl Med.* 2008;49:606–614.
- Krivokapich J, Huang SC, Phelps ME, et al. Estimation of rabbit myocardial metabolic rate for glucose using fluorodeoxyglucose. *Am J Physiol.* 1982;243:H884–H895.
- Feng D, Huang SC, Wang X. Models for computer simulation studies of input functions for tracer kinetic modeling with positron emission tomography. *Int J Biomed Comput.* 1993;32:95–110.
- Hariharan R, Bray M, Ganim R, et al. Fundamental limitations of [<sup>18</sup>F]2-deoxy-2-fluoro-D-glucose for assessing myocardial glucose uptake. *Circulation.* 1995;91:2435–2444.
- Bøtker HE, Bottcher M, Schmitz O, et al. Glucose uptake and lumped constant variability in normal human hearts determined with [<sup>18</sup>F]fluorodeoxyglucose. *J Nucl Cardiol.* 1997;4:125–132.
- Ng CK, Holden JE, Degrado TR, et al. Sensitivity of myocardial fluorodeoxyglucose lumped constant to glucose and insulin. *Am J Physiol.* 1991;260:H593–H603.
- Hashimoto K, Nishimura T, Imahashi KI, et al. Lumped constant for deoxyglucose is decreased when myocardial glucose uptake is enhanced. *Am J Physiol.* 1999;276(1 pt 2):H129–H133.
- Shoghi KI, Gropler RJ, Sharp T, et al. Time course of alterations in myocardial glucose utilization in the Zucker diabetic fatty rat with correlation to gene expression of glucose transporters: a small-animal PET investigation. *J Nucl Med.* 2008;49:1320–1327.
- Shoghi KI, Finck BN, Schechtman KB, et al. In vivo metabolic phenotyping of myocardial substrate metabolism in rodents: differential efficacy of metformin and rosiglitazone monotherapy. *Circ Cardiovasc Imaging.* 2009;2:373–381.
- Wallhaus TR, Taylor M, Degrado TR, et al. Myocardial free fatty acid and glucose use after carvedilol treatment in patients with congestive heart failure. *Circulation.* 2001;103:2441–2446.
- Taegtmeier H, Hems R, Krebs HA. Utilization of energy-providing substrates in the isolated working rat heart. *Biochem J.* 1980;186:701–711.
- Sharma S, Guthrie PH, Chan SS, et al. Glucose phosphorylation is required for insulin-dependent mTOR signalling in the heart. *Cardiovasc Res.* 2007;76:71–80.
- Taegtmeier H. Glucose for the heart: too much of a good thing? *J Am Coll Cardiol.* 2005;46:49–50.
- Taegtmeier H, Dilsizian V. Imaging myocardial metabolism and ischemic memory. *Nat Clin Pract Cardiovasc Med.* 2008;5(suppl 2):S42–S48.
- Goodwin GW, Taylor CS, Taegtmeier H. Regulation of energy metabolism of the heart during acute increase in heart work. *J Biol Chem.* 1998;273:29530–29539.
- Mochizuki T, Tsukamoto E, Ono T, et al. Sequential change of BMIPP uptake with age in spontaneously hypertensive rat model. *Ann Nucl Med.* 1997;11:299–306.
- de las Fuentes L, Herrero P, Peterson LR, et al. Myocardial fatty acid metabolism: independent predictor of left ventricular mass in hypertensive heart disease. *Hypertension.* 2003;41:83–87.
- Wong KP, Sha W, Zhang X, Huang SC. Effects of administration route, dietary condition, and blood glucose level on kinetics and uptake of <sup>18</sup>F-FDG in mice. *J Nucl Med.* 2011;52:800–807.
- Yokoyama I, Inoue Y, Moritan T, et al. Myocardial glucose utilisation in type II diabetes mellitus patients treated with sulphonylurea drugs. *Eur J Nucl Med Mol Imaging.* 2006;33:703–708.
- Bøtker HE, Goodwin GW, Holden JE, et al. Myocardial glucose uptake measured with fluorodeoxyglucose: a proposed method to account for variable lumped constants. *J Nucl Med.* 1999;40:1186–1196.
- Wiggers H, Bottcher M, Nielsen TT, et al. Measurement of myocardial glucose uptake in patients with ischemic cardiomyopathy: application of a new quantitative method using regional tracer kinetic information. *J Nucl Med.* 1999;40:1292–1300.
- Herrero P, Sharp TL, Dence C, et al. Comparison of <sup>1-11</sup>C-glucose and <sup>18</sup>F-FDG for quantifying myocardial glucose use with PET. *J Nucl Med.* 2002;43:1530–1541.
- Nakamoto M, Ohya Y, Shinzato T, et al. Pioglitazone, a thiazolidinedione derivative, attenuates left ventricular hypertrophy and fibrosis in salt-sensitive hypertension. *Hypertens Res.* 2008;31:353–361.